Normal and Lateral Interactions between Thermosensitive Nanoparticle Monolayers in Water

Xavier Banquy,[†] Eric Charrault,[‡] and Suzanne Giasson*[,†,‡]

Faculty of Pharmacy and Department of Chemistry, University of Montréal, C.P. 6128, succursale Centre-ville, Montréal, Québec, Canada H3C 3J7

Received: November 18, 2009; Revised Manuscript Received: April 16, 2010

Static and dynamic interaction forces between two thermosensitive polymeric nanoparticle monolayers grafted onto mica surfaces and immersed in water were studied using a surface forces apparatus. The polymeric nanoparticles (NPs) were made of *N*,*N*-diethylacrylamide and had a hydrodynamic diameter of ca. 780 nm at 20 °C in aqueous suspension. They were irreversibly grafted onto chemically modified mica surfaces at a constant surface coverage of 2.6 NPs/μm^2. The measured normal forces between two opposing NP monolayers were found to be strongly dependent on the temperature. At temperatures lower than the lower critical solution temperature (LCST), the grafted NPs were swollen, and the normal interaction forces between the two NP monolayers were repulsive. Above the LCST, the NPs collapsed, and attractive forces between the NP layers were measured. The swollen NPs were found to exhibit very low friction forces compared to the collapsed ones. The effect of the sliding velocity on the shear stress was investigated, and the results are in agreement with the so-called adhesive friction model developed for rubber friction. Our results suggest that the water content in the contact area and the interdiffusion of polymer chains are important parameters in determining the friction between polymer-bearing surfaces.

Introduction

A large number of materials directed toward the control of interfacial properties have been developed in the past several years for applications such as biosensors, lubricants, nanolithography, and micromechanical devices.[1–4] Their design generally requires a fine-tuning of the physical properties of the surface layer on the atomic scale to control the surface response under different environmental conditions. Grafted or self-adsorbed polymers have demonstrated the ability to respond to very subtle changes in properties of the surrounding medium such as pH,[5] temperature,[6] ionic strength, and solvent quality.[7,8] Upon the application of stimuli, polymer layers can undergo molecular conformational changes that, in turn, affect macroscopic properties such as adhesion, lubrication, friction, and wettability of surfaces.[9,10]

The use of stimuli-responsive polymers as lubricants has a strong potential for biotechnological applications in tissue engineering and biolubrication. The good lubricating properties of end-grafted polymer layers or polymer brushes have been shown to be associated with the fluidity of the solvent trapped between the surfaces or the effective viscosity of the sheared layer,[11–13] the strong osmotic pressure supporting the load between the surfaces,[14,15] and the small extent of mutual interpenetration or low adhesion between the two opposing polymer layers.[16] Mutual interpenetration of polymer chains from one surface to the other is believed to be the main contribution to the total friction force between polymer-bearing surfaces.[17] The extent of the interpenetration zone depends on the solvent quality, the grafting density, the presence of electrostatic interactions between and within the polymer layers, and the applied load or pressure between the two opposing polymer layers.[16–19] Two opposing polymer layers made of cross-linked polymer are expected to exhibit very low levels of mutual interpenetration because of the restricted number and length of free dangling chain ends exposed at the polymer surface. Indeed, friction forces between hydrogel surfaces have been shown to be relatively low under pressure of ca. 0.1 MPa.[20]

Even though polymer brushes have shown to exhibit very good lubricating properties, the mechanism underlying the friction dissipation is still unclear mainly because of the difficulty in controlling polymer grafting density on a mica surface, which is the most reliable substrate for accurate force measurements using a surface forces apparatus (SFA). Most of the reported studies on polymer-mediated lubrication using SFA involve physisorbed polymers or physisorbed macroinitiors,[14,15] which are susceptible to desorption, or cleavage, under changes in environmental conditions (i.e., pH, ionic strength, applied load, and shear). A recent study using irreversibly attached charged polymer brushes showed that the friction forces were not as low as had previously been reported for physisorbed highly charged brushes of similar molecular weight and grafting density.[21] This study suggested that the role of the electrostatic interactions in controlling friction is to control the thickness of the mutual interpenetration zone over which friction dissipation occurs. In addition, the friction forces measured under large applied loads and high shear rates were not found to be associated with polymer cleavage or surface damage (or wear) as frequently observed with physisorbed polymers.[21]

In this study, we present the tribological behavior of two opposing polymeric monolayers made of thermosensitive hydrogel nanoparticles (NPs) covalently attached to mica surfaces. The NPs are made of crosslinked polymer in order to prevent mutual interpenetration of dangling chains as previously men-

* To whom correspondence should be addressed. E-mail: suzanne.giasson@umontreal.ca. Tel.: 514 340 5175. Fax: 514 340 5290.
[†] Faculty of Pharmacy.
[‡] Department of Chemistry.

10.1021/jp910965p
Published on Web 07/09/2010

tioned. The normal and lateral forces between two symmetrical monolayers were measured in water at different temperatures. The effect of the NP conformation (i.e., swollen and collapsed states) on the interaction forces is discussed and analyzed in the framework of the so-called adhesive friction model for multicontact interfaces.

Materials and Methods

General. Ruby mica sheets were purchased from S&J Trading Inc. (Glen Oaks, NY). Plasma Prep II from SPI Supplies was used to activate the mica surfaces using argon (5.0 grade) and Milli-Q-quality water. Aminopropyltriethoxysilane (APTES), glutaraldehyde [25% (w/w) in water], 2-hydroxyethyl methacrylate (HEMA), bisacrylamide (BisA), and sodium cyanoborohydride ($NaBH_3CN$, 5 M in 1 M NaOH aqueous solution) were purchased from Aldrich. Sodium dodecyl sulfate (SDS) and potassium persulfate (KPS) were obtained from Fluka. Milli-Q-quality water was obtained from a Millipore Gradient A 10 purification system [resistance 18.2 MΩ·cm, total organic carbon (TOC) = 4 ppb].

Synthesis of Nanoparticles. *N*,*N*-Diethylacrylamide (DEA) and the nanoparticles were synthesized as described elsewhere.[27] Briefly, the monomers (90 mol % DEA and 10 mol % HEMA; total amount of 26.5 mM in water), BisA (1.5 mol %), and SDS (0.040 g) were added to 200 mL of Milli-Q water under stirring, and the mixture was then purged with nitrogen for 30 min at 70 °C. KPS (0.120 g) dissolved in 15 mL of Milli-Q water was added to the solution. The reaction was allowed to proceed for 4 h, and the system was subsequently cooled to room temperature before the milky suspension was filtered through 2.0-μm Millipore Isopore membrane filters. The filtrate was centrifuged for 40 min at about 15000 rpm. The polymer particles were collected and purified by dialysis for 1 week in Milli-Q water. NPs synthesized by this protocol have a mean diameter of 780 nm in water at 20 °C as measured by dynamic light scattering (DLS).[22] The lower critical solution temperature (LCST) below which the NPs are expected to be in a collapsed conformation is ca. 23 °C, as previously reported.[22]

Reactive Layer Preparation. All surface manipulations were performed in a clean laminar-air-flow cabinet to prevent dust deposition on the surfaces. All glassware was carefully cleaned in a bath of saturated potassium hydroxide/isopropyl alcohol and then intensively rinsed with Milli-Q water.

Grafting of APTES onto OH-activated mica surfaces performed as already reported.[23,24] Mica surfaces were placed in a plasma chamber and under a vacuum pressure of 0.5 mTorr. Argon gas and water vapors were then introduced at partial pressures of 80 and 300 mTorr, respectively. Plasma activation was performed for 5 min at 40 W, and then, the mica surfaces were left in the plasma chamber under vacuum (0.5 mTorr) for another 5 min before they were transferred into an evaporation chamber and stored under vacuum (1.6 mmHg) prior to the APTES grafting reaction. The evaporation chamber was connected through a valve to a small glass reservoir containing 100 μL of APTES. The OH-activated mica surfaces were kept in the chamber under vacuum for 15 min and then, the valve was opened allowing APTES vapor to react with the surface hydroxyl groups. During this step, vacuum was maintained to ensure a constant flux of APTES vapor into the chamber and to avoid condensation of APTES on the activated mica surfaces. Evaporation was allowed to proceed for 4 h. The valve was then closed and remnant APTES vapor was pumped out for 2 h. APTES covalent grafting was completed by annealing the surfaces for 30 min at 120 °C under atmospheric pressure. Then, the surfaces bearing the grafted APTES molecules were immersed in a 1% (w/w) water solution of glutaraldehyde overnight, during which time a coupling reaction between the APTES amine function and the glutaraldehyde carbonyl function took place[25,26] in the presence of $NaBH_3CN$.[25,26] The resulting glutaraldehyde-functionalized mica surfaces (Glu-surfaces) were thoroughly rinsed with Milli-Q water prior to nanoparticle deposition.

Nanoparticle Deposition. Nanoparticle deposition was performed using the horizontal convective evaporation method.[27,28] Glass coverslips were cleaned in a piranha solution [H_2O_2/H_2SO_4 30/70 (v/v)] at 40 °C for 40 min and thoroughly rinsed with Milli-Q water. Glu-surfaces were placed under a clean glass coverslip applicator at an angle of 15°. The separation distance between the applicator and the Glu-surfaces was kept constant during the deposition process (between 50 and 150 μm). Prior to translation of the Glu-surface, a drop (25 μL) of a 0.1% (w/w) NP suspension was placed between the applicator and the surface. As the Glu-surface was translated at a fixed velocity of 11 μm/s, the suspension drop spread on the substrate, forming a uniform thin film of NPs. The deposition process was performed on a vibration-isolated table in a closed sealed box at constant temperature (24 °C) and constant relative humidity (30 ± 3%).

Surface Forces Measurements. ***Normal Interaction Forces.*** The interaction forces between two NP monolayers were measured as a function of the separation distance using the SFA2000 surface forces apparatus. Briefly, the SFA enables the force as a function of surface separation D between two curved surfaces to be determined by measuring the deflection of a double cantilever spring that supports the lower surface. The distance between the back-silvered mica substrates is measured by an interferometry technique that uses fringes of equal chromatic order (FECO).[29] The measured normal force, F_N, between the cylindrically curved surfaces can be expressed in terms of free energy of interaction per unit area between two infinite flat surfaces, E, using the Derjaguin approximation $F_N/R = 2\pi E$, where R is the surface curvature.[30]

Back-silvered mica surfaces were glued silver side down on the SFA's cylindrical disks (curvature of 2 cm) using Norland 81 UV cured glue. The two disks were mounted in the SFA chamber in a cross-cylinder geometry and were brought into adhesive contact in air to set the contact separation distance $D = 0$ between the two mica surfaces. The SFA disks were then dismounted under a laminar-flow cabinet for surface modification and NP deposition. Once the functionalized layer (APTES + glutaraldehyde) was grafted onto the OH-activated mica, the surfaces were mounted back in the SFA chamber and brought into adhesive contact in air to determine the thickness of the functionalizing layer. The reference distance reported for the force profiles ($D = 0$) was arbitrarily set as the adhesive contact distance between two Glu-surfaces in air. The surfaces were dismounted again for NP deposition and mounted back at a separation distance of approximately 0.5 mm. A small droplet of pure water was introduced between the two NP-covered surfaces, and the bottom of the SFA chamber was covered with water to minimize water evaporation from between the two surfaces. The SFA chamber was sealed from the experimental by room, whose temperature was precisely controlled, and allowed to equilibrate over 12 h. The final configuration of the system consisted of two facing mica surfaces bearing one grafted NP monolayer each, with similar surface coverage. The normal interaction forces between the two surfaces as a function of the separation distance, $F_N(D)$, was determined by changing the

separation distance between the surfaces in a stepwise manner (ca. 6 nm for each step). The separation distance was changed at a velocity of ca. 3 nm/s. The time required for the surface separation distance to equilibrate between each step (i.e., for a change in D less than 0.4 nm/min at rest) was approximately 60 s. The force profiles are presented as the normal interaction force normalized by the surface curvature or as the direct measured force as a function of separation distance.

Friction Force Measurements. The lateral force, or friction force, was measured by displacing the upper surface horizontally using a piezo-driven sliding device. The velocity of this device was computer-controlled and calibrated before each experiment using a laser displacement detection device (Keyence, Canada) with a resolution of 10 nm. The upper surface was connected to a vertical cantilever spring whose lateral deflection allowed friction force to be measured using strain gauges. The resolution in measuring friction force was 10^{-3} mN, and the signal noise was lower than 1×10^{-3} mN. In our experiments, the lateral sliding speed was varied from 0.02 to 1 μm/s. Before the friction forces were measured, three normal force profiles were performed on the same contact position to ensure the reversibility and reproducibility of the behavior of the NPs under compression. Friction forces were measured on two different pairs of surfaces with an average of three contact points on each pair.

Atomic Force Microscopy (AFM). AFM imaging was carried out using a Multimode Dimension 3100 atomic force microscope and a NanoScope IIIa controller (Digital Instruments) operated in tapping mode using aluminum-coated silicon tips from NanoWorld (ARROW-NCR-20). Data analysis was performed using the NanoScope III software (version 5.30r3). All images were taken at 25 °C and 30% relative humidity. To measure the surface coverage of the NPs on the surfaces, 10 images (30×30 μm) were captured on each surface before and after measurement of the interaction forces to observe whether any surface damage occurred during the surface forces measurements. During the SFA experiments, a magnified top view of the contact was obtained by adding a camera and viewing eyepiece above the objective lens used to focus and collect the light coming out of the interferometer. When possible, particular features close to the contact point were arbitrarily chosen as the contact reference for AFM imaging.

Results and Discussion

Normal Forces between Two NP Monolayers Grafted onto Mica Surfaces. The normal interaction forces between two NP monolayers as a function of separation distance were measured below and above the LCST (i.e., ca. 23 °C). AFM imaging was carried out before and after the force measurements. The image analysis showed that the NP surface density remained constant and that the NP monolayers did not suffer any damage during force measurements for temperatures ranging from 15 to 30 °C (data not shown). Typical AFM images of these grafted NP monolayers were previously reported.[24] In addition, the force profiles measured on bringing together and separating the surfaces were reproducible and did not show any significant hysteresis or history effect (Figure 1). These observations are consistent with the covalent attachment of the NPs preventing their detachment or desorption from the surfaces upon changes in environmental conditions (i.e., temperature, compression). However, hysteresis and history effects were observed in the force profiles measured in air (previous results reported in Figure 1).[24] These effects were ascribed to plastic deformation of the dry NPs upon compression.

The force profiles measured at different temperatures ranging from 15 to 30 °C are illustrated in Figure 2. Because the NP

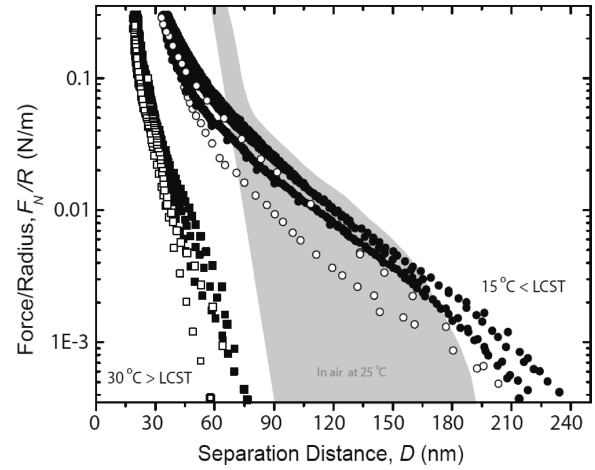

Figure 1. Normalized interaction forces measured between two opposing NP monolayers in water as a function of the separation distance D between the functionalized surfaces and at temperature above (squares) and below (circles) the LCST of the NPs. $D = 0$ refers to the adhesive contact, measured in air at RT, between two glutaraldehyde-functionalized mica surfaces which are the substrates for the grafted NPs. The force profiles were measured on decreasing D (filled symbols) and increasing D (empty symbols). Also shown, the large hysteretic area for the first force profile measured between the NP monolayers in air at 25 °C.[24]

grafting density remained constant with changing temperature, the changes in the force profiles are due solely to changes in particle conformation upon change in temperature. The interaction profiles were reversible and entirely repulsive for temperatures $\leq$ 25 °C. However, an attractive force regime was observed at $T = 30$ °C, which is above the LCST (Figure 2b), as expected between polymer segments in bad-solvent conditions. The attractive regime did not exhibit any hysteresis and/or history effect. Because the NPs do not carry any significant effective electric charge on their surface,[31] the long-range repulsive forces measured at $T \leq 25$ °C are expected to be governed by the osmotic repulsion between polymer segments and to occur at separation distances corresponding approximately to the physical contact between the two opposing NP monolayers. Therefore, the thickness of two opposing unperturbed NP monolayers was chosen as the onset of repulsive interactions. This onset of interactions was arbitrarily set as the distance for which the interaction force became larger than 1 mN/m on decreasing separation distance, with 1 mN/m corresponding to negligible interactions within the experimental error at large separation distances. As shown in Figure 2, the onset of interactions decreases from ~225 to ~70 nm as the temperature increased from 15 to 25 °C (or the solvent quality decreases), corresponding to monolayer thickness ranging from ~113 to ~35 nm, which are considerably smaller than the size of the particles dispersed in water at 20 °C (ca. 780 nm).[22] These force profiles, together with the AFM analysis previously reported for these systems,[24,31] clearly indicate that the NPs are significantly deformed on the surfaces even under no or negligible applied load. Such a deformation is known to occur with hydrogel particles deposited on flat surfaces, especially if the particles contain very low amounts of cross-linking agent, as reported by Wiedemair et al.[32]

The capacity of the particles to deform could explain the long-range attractive regime measured at 30 °C. The attractive well is relatively small (2.5−3 mN/m) and is located at ca. 62 nm. Figure 3 illustrates a possible scenario for particle deformation as the separation distance is decreased between the surfaces.

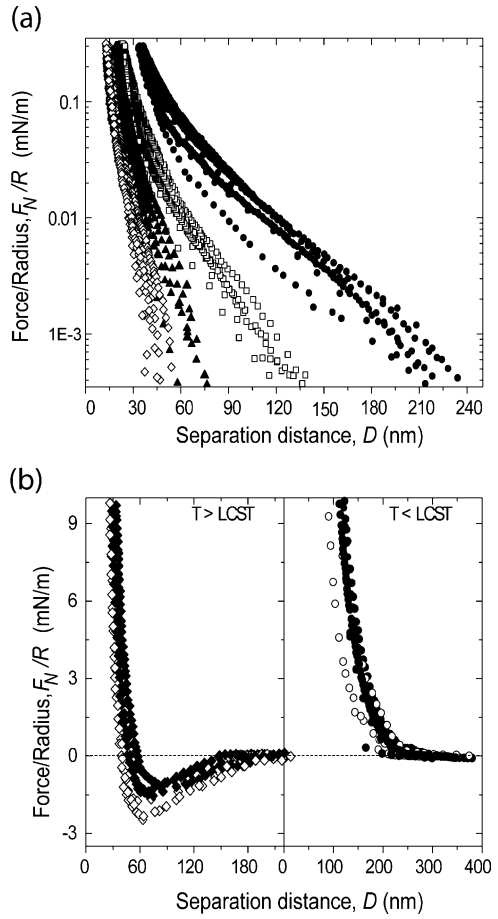

Figure 2. (a) Normalized interaction forces as a function of the separation distance D between two opposing NP monolayers in water at different temperatures; ●: 15 °C, □: 20 °C, ▲: 25 °C, ◇: 30 °C. Force profiles measured on decreasing and increasing D for a same contact point are illustrated using the same symbols as no significant hysteresis was observed in the repulsive regime. (b) Amplified view of the force profiles measured at: ● ○, 15 °C (<LCST); 30 °C (>LCST). Filled and empty symbols represent the force profiles measured on decreasing and increasing D respectively to illustrate the hysteresis in the attractive regime.

Assuming that the equilibrium contact between the opposing NP monolayers occurs at zero force between the NP layers (point D in Figure 3 corresponding to a separation distance of ca 55 nm), the thickness of a NP monolayer in the collapsed state would correspond to approximately 27 nm, which is smaller than the unperturbed thickness of the NP monolayer measured from the onset of interactions at 25 °C (i.e., ca. 35 nm) and consistent with the collapse of the particles as the temperature increases. However, the estimated monolayer thickness is significantly smaller than the size of the NPs dispersed in water at 30 °C (ca. 200−300 nm),[22] which suggests that the NPs can also deform significantly on surfaces even in a collapsed conformation. These observations are consistent with the fact that these hydrogel NPs have a low elastic modulus at 37 °C (Young's modulus < 1 MPa)[31] and that multiple covalent bonds can be formed with the substrate, thus promoting particle deformation. Such deformation has also been observed with poly(*N*-isopropylacrylamide) (PNIPAM) particles deposited on mica surfaces in water.[32,33] The capacity of hydrogel particles to deform even in a bad solvent could explain the large deformation of the opposing NP monolayers (i.e., from a thickness of ∼27 to ∼75 nm) under the influence of attractive segment−segment interactions (Figure 3).

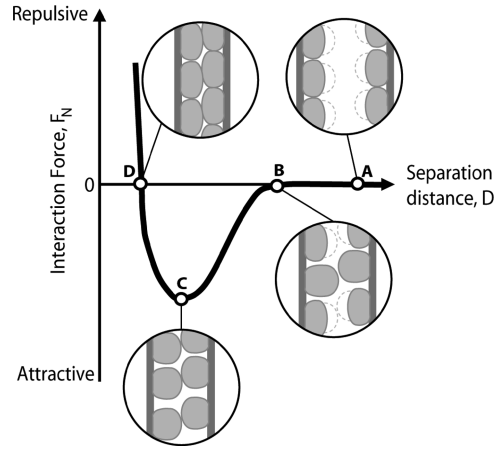

Figure 3. Schematic illustration of the interaction forces between NP monolayers in the collapsed state. The surface coverage of the NPs is 2.63 NPs/μm^2 and corresponds to high surface coverage. D corresponds to the separation distance between the two opposed faces of the functionalized mica surfaces. At large D (point A), interaction forces are negligible (below the detection limit of the measuring device). From B to C, segment−segment attractive forces arise from the opposing and deformed (stretched) NPs; from C to D, interdiffusion occurs between the superficial free polymer chains, and the osmotic pressure increases as the separation distance is decreased; from point D to D = 0, osmotic repulsion associated with the compression of the NP monolayers prevails.

The slope of the F_N versus D curves illustrated in Figure 2 (dF_N/dD) can be used to estimate the relative elasticity of the NP monolayers. As the NPs are collapsing with increasing temperature, they are also expected to become more elastic because of the increase in the polymer volume fraction within their network. Indeed, the hydrogel NPs showed a 17-fold increase in elasticity with a 15 °C increase in temperature (from 15 to 30 °C). This is in relatively good agreement with the reported 10- to 15-fold increase in the Young's modulus for a PNIPAM nanoparticle undergoing a transition from swollen to collapsed state.[32−34] In comparison, the elasticity of the NPs in air at 25 °C is 4 times smaller than that observed in the collapsed state at 30 °C.[24]

Lateral Forces between NP Monolayers. The friction forces between two NP monolayers grafted onto mica surfaces sliding past each other were first measured at a constant sliding velocity (100 nm/m) as a function of applied load, and at temperatures of 15 and 30 °C. Figure 4 reports the kinetic friction force, F_k, which corresponds to the friction force observed during steady-state sliding. The results show a linear relationship between F_k and the applied load (or normal force) F_N up to a load corresponding to pressures of 3.5 and 5 MPa at 30 and 15 °C, respectively (Figure 4). Within this linear regime, a friction coefficient μ can be determined according to Amonton's law

$$\mu = \frac{dF_k}{dF_N} \quad (1)$$

resulting in values of 0.04 ± 0.01 at 15 °C and 0.26 ± 0.01 at 30 °C. The friction coefficient measured between the NP monolayers in the swollen state (15 °C) is similar to values generally reported for polymer brushes in good solvents at low applied pressures (below 1 atm).[14,35] However, whereas end-grafted polymers usually exhibit a significant increase in friction coefficient at higher loads, the friction between the swollen NP monolayers remained relatively low up to pressure 1 order of

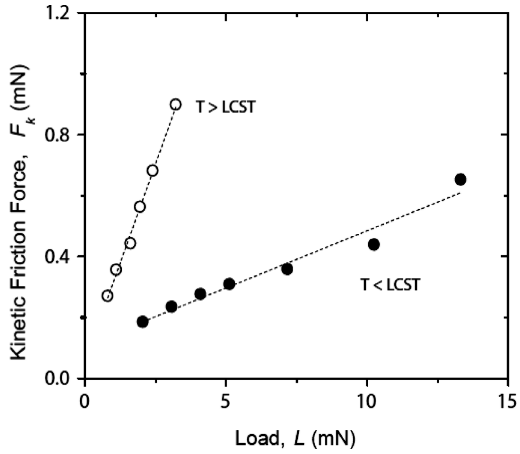

Figure 4. Kinetic friction force measured between two NP monolayers as a function of applied load. Measurements were performed at a sliding velocity of 100 nm/s and at 15 °C (empty circles) and 30 °C (filled circles). The friction coefficient μ calculated according to Amonton's law corresponds to 0.04 ± 0.01 for T = 15 °C (<LCST) and 0.26 ± 0.01 for T = 30 °C (>LCST).

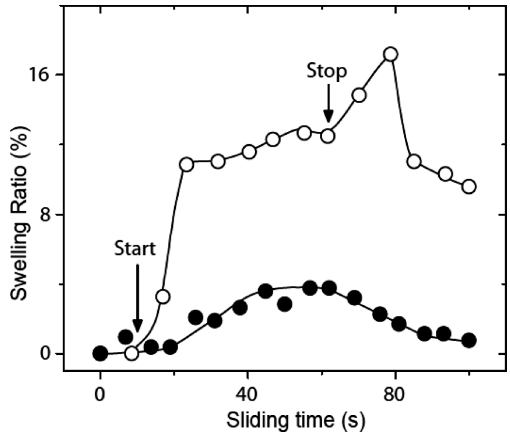

Figure 5. Evolution of the swelling ratio of the NP monolayers as they slide past each other at a sliding velocity of 660 nm/s and under a normal applied load of ca 2 mN. The sliding was performed for 50 s. The swelling ratio corresponds to $(D_t - D_{rest})/D_{rest}$ where D_t and D_{rest} correspond the separation distance during sliding and at rest respectively. The experiments were performed on the same contact area.

magnitude larger than the maximum pressure that self-adsorbed polymer brushes can generally sustain. This is explained by the fact that the NPs were covalently attached to the substrates, allowing higher pressures to be sustained by the sheared polymer layers, whereas physisorbed polymer brushes are susceptible to desorption under shear and applied loads.

Our data also show a shear-induced swelling of the NPs. The change in particle size induced by shearing was quantified by a swelling ratio defined as $(D_t - D_{rest})/D_{rest}$, where D_t and D_{rest} correspond to the separation distance during sliding and at rest, respectively. As shown in Figure 5, very low swelling ratios (< 4) are observed at 30 °C, but significant swelling (> 12) appears at 15 °C as also observed for grafted polymeric chains in good solvents under a shear flow.[36]

The higher friction coefficient observed for the collapsed NPs can be partially attributed to the presence of attractive forces between the NP monolayers (Figure 2). The 7-fold increase in the friction coefficient from the swollen state to the collapsed state is of the same order of magnitude as the values reported for thermosensitive and pH-sensitive grafted brushes undergoing similar conformational transitions.[37]

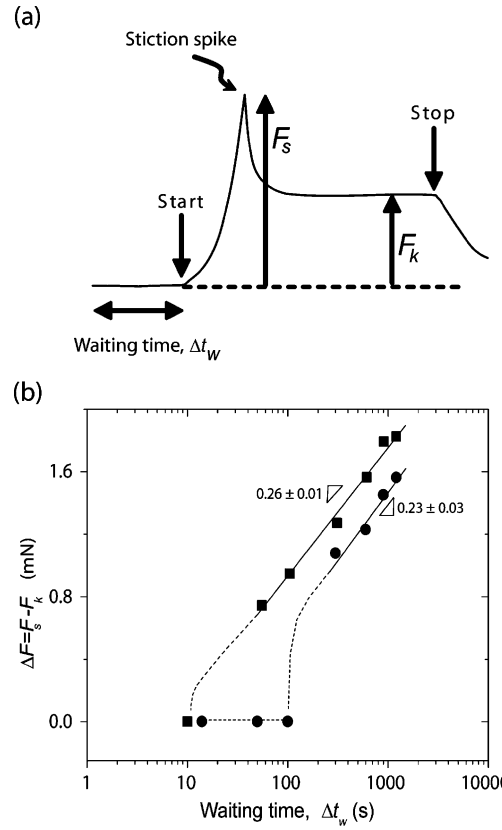

Figure 6. (a) Representation of the start-and-stop experiments. The two NP-coated surfaces are first brought into contact under an applied load of 1.8 mN and allowed to equilibrate for a given amount of time, Δt_w. After this time, the upper surface is moved laterally at a fixed velocity for a time Δt. During this time, the friction force increases from 0, which corresponds to the resting state, to a maximum corresponding to the static friction force F_s and decreases to reach the steady-state kinetic friction force F_k. (b) Evolution of $F_s - F_k$ with resting time at contact Δt_w. Circles and squares represent measurements done at T = 30 °C (>LCST) and T = 15 °C (<LCST), respectively.

To get more insight into the friction mechanism, the effects of the contact time and the sliding velocity on the friction forces were analyzed. The effect of contact time was investigated by performing "start-and-stop" experiments at a constant driving velocity of 100 nm/s and under an applied load of 1.8 mN, as illustrated in Figure 6a. Above a certain critical contact time, a spike in static friction preceded the steady-state or smooth-sliding regime. The static friction force, F_s (threshold of relative motion), corresponds to the maximum of the stiction spike. The difference between the static and kinetic frictions, $F_s - F_k$, is reported as a function of contact time in Figure 6b. In both conformational states, the dependence of $F_s - F_k$ on contact time can be described by a power law as $F_s - F_k \approx a(\Delta t_w)^b$, where a is a prefactor. The exponent b corresponds to 0.26 ± 0.01 and 0.23 ± 0.03 for the swollen and collapsed states, respectively. Both values are similar to the characteristic exponent predicted for a polymer interdiffusion process (i.e., 0.25),[38] suggesting that polymer chains from one NP monolayer, most probably the free dangling chain ends, might diffuse and entangle within the polymer network of the opposing NP monolayer. The results presented in Figure 6b could also be fitted with a logarithmic law (data not shown) formulated in terms of a slow increase in contact area under shear or a stiffening of the contact at rest due to the thermally activated relaxation of local stressed zones in the contact region. Logarithmic models generally consider an increase in contact

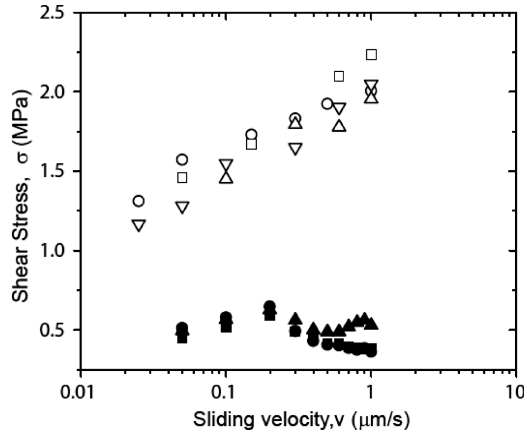

Figure 7. Shear stress between two opposing NP monolayers as a function of sliding velocity and for different applied loads. Open symbols correspond to experiments carried out at $T = 30$ °C (>LCST) under different loads (Δ, 0.8 mN; □, 1.1 mN; ○, 1.6 mN; ∇, 3.2 mN), and filled symbols correspond to experiments carried out at $T = 15$ °C (<LCST) and different loads (●, 0.6 mN; ■, 1.2 mN; ▲, 1.8 mN).

area between asperities with increasing contact time or shear. As the change in real contact area could not be directly measured and as no significant change in the apparent contact area could be detected during rest or shearing, this adhesion-friction mechanism underlying the logarithm law was not used to analyze and interpret our experimental data.

The critical contact time between the collapsed NPs was twice that obtained for the swollen NPs, namely, 100 and 50 s, respectively (Figure 6b). This difference can be associated with different chain mobility and interdiffusion kinetics expected for different solvent qualities. When the NPs are in a swollen conformation, the diffusion of the free chain ends is promoted by the favorable interactions between the polymer and the solvent. In the collapsed state of the NPs, the interactions between polymer and solvent are disfavored and prevent diffusion of the chains thought the solvent.

The variation in the kinetic friction force measured between two opposing NP monolayers, F_k, as a function of sliding velocity, v, is illustrated in Figure 7 for various applied loads at 15 and 30 °C. The friction is expressed in terms of shear stress, $\sigma = F_k/A$, where A is the contact area. The contact area was assumed to be the apparent contact area, which was measured in real time during sliding using the interferometry technique. The sliding or driving velocity, v, was varied from 20 nm/s to 1 μm/s. Above a velocity of 1 μm/s, surface damage was episodically observed and the measured friction forces were hardly reproducible. Therefore, these data are not reported in Figure 7. In the load interval studied (from 0.8 to 3.2 mN), the contact area appeared to vary linearly from ca. 300 to 1700 μm^2 with the applied load (data not shown). Within the experimental error and under the experimental conditions used, the $\sigma-v$ curves are independent of the applied load but strongly dependent on the conformation of the NPs. In the collapsed state, the shear stress increases with the logarithm of the sliding velocity, as is commonly observed in lubricated contacts.[39–41] In the swollen state, two regimes were observed: a logarithmic increase in shear stress with the sliding velocity at low sliding velocities and a decrease in σ with v^{-1} at higher velocities. A maximum in the $\sigma-v$ curve occurred at a sliding velocity of ca. 0.2 μm/s. Rolling of the sheared NPs is precluded because the NPs were covalently attached to the substrate. The existence of a maximum in the $\sigma-v$ curve has previously been reported in tribological studies of soft layers such as alkyl thiols grafted on gold substrate,[42] surfactant monolayers,[43,44] and hydrogels.[45] Theoretical explanations of this behavior have been proposed,[43,46,47] involving arguments of the adhesive friction model developed for rubberlike materials by Schallamach.[48] According to this model,[43] the two contacting surfaces interact primarily through small adhesive domains, which can be called junctions. During sliding, these junctions are continually formed and broken. A junction can be broken by two main mechanisms: by thermal excitation or by an applied shear force. At rest (no applied shear), the junction remains in the bound state for an average time of τ_0 and spontaneously breaks under thermal fluctuation. After a time τ_f, the junction spontaneously re-forms by the same thermal process. Upon sliding, the bound junctions are deformed elastically, which reduces the energetic barrier to break the junction and consequently decreases the lifetime of the junction to τ_b. A junction can also be broken once the deformation reaches the yield point characterized by the critical deformation l. Different frictional regimes are predicted by this adhesive junction model. At very low sliding velocity, $v \ll l/\tau_0$, the applied shear force does not contribute to the breaking of the junctions in the adhesive state and therefore, the resulting shear stress is directly proportional to the sliding velocity. At higher velocity, when v becomes comparable to l/τ_0, both the thermal and forced rupture mechanisms are involved. In this regime, the predicted relationship between the shear stress and the sliding velocity is[49]

$$\sigma \approx \frac{1}{2}\frac{k_B T}{V_a}\ln\left(\frac{v}{v_0}\right) \tag{2}$$

where V_a represents the activation volume and v_0 is a reference velocity.

At much higher velocity, when $v \gg l/\tau_f$, the number of adhesive junctions decreases with increasing sliding velocity, and the shear stress is[49]

$$\sigma \approx \frac{1}{2v\tau_f}N\frac{\delta A}{d}Gl \tag{3}$$

where N represents the total number of junctions per unit surface area, d is the junction thickness, G is the shear modulus, and δA is the surface area of one junction. If τ_0 and τ_f are sufficiently different, an intermediate regime can appear when $l/\tau_f \gg v \gg l/\tau_0$. In this regime, the junctions are elastically broken as they reach the critical deformation and then, the shear stress is independent of v. The shape of the $\sigma-v$ curve depends strongly on the respective values of τ_0 and τ_f.[43] When the condition $\tau_0 > \tau_f$ does not hold, the logarithmic and v^{-1} regimes can fuse and leave only one peak in the $\sigma-v$ curve.

Our experimental results can be well described by this adhesive junction model. Dangling chains located mainly at the NP surface most probably form the adhesion sites. The existence of the maximum $\sigma-v$ curve for the swollen NPs corresponds to the crossover of the purely elastic friction regime, which is described by eq 2, and the nonadsorbing regime described by eq 3. According to the adhesive friction model developed by Gong et al.,[47] the velocity at the maximum scales as $v_m \approx T^{1/3}E^{2/3}/\eta$, where T is the temperature, E is the Young's modulus of the gel, and η is the viscosity of the solvent. As observed by the slope of the F_N vs D curves in Figure 2a, the effective stiffness of the NPs increases by one order of magnitude when

temperature increases from 15 to 30 °C. Therefore, v_m in the collapsed state is expected to be 5 times larger than that in the swollen state which is far from of our experimental conditions. This could explain the absence of a maximum in the $\sigma - v$ curve for the NPs in the collapsed state.

The results presented in Figure 7 (shear force versus velocity) could most probably also be fitted with a logarithmic law formulated in terms of thermally activated relaxation of local stressed zones based on the Tomlinson model. Indeed, the presence of a characteristic restoring time for a deformed asperity to recover the nonstressed state would imply a maximum in the friction force versus velocity curve. The data illustrated in Figure 6 suggest that the longer the critical time, the smaller the restoring time (time for the chains to relax or desentangle). The fact that the restoring time of the NPs below the LCST is longer than that of the collapsed state (above the LCST) could then explain the presence of a maximum in the sliding curve for the former case. Nevertheless, in the absence of a study of single-particle rheology, this mechanism cannot be easily elucidated. In addition, the interpretation of our data using the adhesive junction model does not invalidate the importance and the conclusions of our study.

Assuming that the adhesive junction model provides a good physical model for the tribological behavior of the NPs, the activation volume of the adhesive junctions can be estimated by fitting eq 2 to the experimental data shown in Figure 7 in the logarithmic regime. The activation volume corresponds to an equivalent sphere of 5-nm diameter for the collapsed state and 7-nm diameter for the swollen state. Both values are well below the diameter of the NPs but seem to scale with the size of a macromolecule. These results, together with the effect of the contact time on the friction forces, support the assumption that friction is mainly due to the elastic dissipation generated from the detachment and/or disentanglement of the superficial polymer chains forming adhesive junctions between the opposing NPs.

The effect of temperature on the conformation of the opposing hydrogel NP monolayers and on the resulting frictional behavior is schematically illustrated in Figure 8. The collapse of the NPs with increasing temperature is associated with an increase in the NP elasticity and an insignificant swelling of the NPs during sliding, suggesting that the presence of water in the contact area is considerably reduced compared to the swollen state. Dehydration of the polymer network in the contact zone favors the contact between polymer chains but does not necessarily promote chain interpenetration. As shown in Figure 6b, the onset of static friction is delayed (in terms of contact time) in the collapsed state compared to the swollen state. This might be due to the relatively slow interdiffusion process of the mobile chains in the collapsed polymer network. However, the collapsed chains are able to store and release more elastic energy than the swollen conformation and therefore give rise to higher kinetic friction. The swollen mobile chain ends can diffuse faster in the opposing surface and they store less elastic energy upon stretching. In addition, the presence of water molecules around the swollen polymer network most probably promotes sliding, as the viscous dissipation associated with water is expected to be negligible within the range of sliding velocities used in this study.

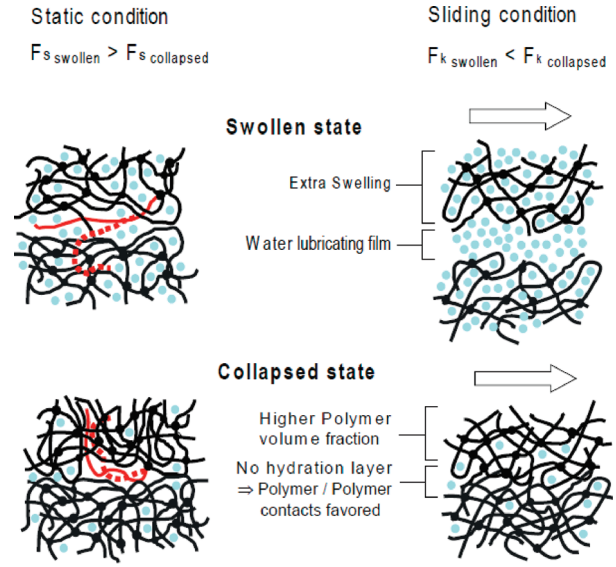

Figure 8. Schematic illustrations of possible conformations for two opposing NP monolayers under static and dynamic interactions. Under static conditions (no sliding), a constant normal load is applied to maintain the two opposing NP monolayers into contact. In the swollen state, free chain ends from one NP monolayer can diffuse (dotted line) easily and form entanglements in the polymer network of the opposing NP monolayer. As a result, the static friction force increases rapidly with contacting time. In the collapsed state, the free chain ends are most probably buried within the NPs and diffuse much more slowly than in the swollen state. Under dynamic conditions (sliding), shear induces swelling below LCST suggests the presence of a thin water film between the two opposing NP monolayers which can favor the lubrication within the sliding interface. In the collapsed state, multiple adhesive junctions between opposing NPs promote energy dissipation during shear.

Conclusions

The adhesion and friction behavior of hydrogel nanoparticle (NP) monolayers covalently attached to mica surfaces and immersed in water was investigated. We showed that the thermosensitivy of the NPs covalently attached to a substrate is preserved. For temperatures below the LCST, two opposing NP monolayers exhibit a purely repulsive normal force profile, which is associated with very low friction forces. The friction coefficient between the swollen NP monolayers remained significantly low (ca. 0.04) up to a pressure of 5 MPa. In their collapsed state (i.e., for temperatures above the LCST), the opposing NP monolayers were found to be slightly attractive, and the resulting friction coefficient is significantly larger (0.26) than that measured in the swollen state.

The study of the variation in the kinetic friction force with the sliding velocity and contact time showed that the friction between the NP monolayers can be well described by the adhesive junction model and mainly depends on the extent of interdiffusion of the superficial polymer chains and elastic adhesive junctions between the particles.

The covalent attachment of the nanoparticles to the substrate ensured that conformational responses to external stimuli (i.e., temperature, compression, shear) were reversible. The control of surface properties using such materials represents an important issue for the development of stimuli-responsive surfaces.

Acknowledgment. This work was supported by the Natural Sciences and Engineering Research Council (NSERC). We thank X. X. Zhu and Carlos Drummond for fruitful discussions and R. E. Prud'homme for providing access to his AFM facilities.

References and Notes

(1) Sliney, H. E. *Tribol. Int.* **1982**, *15*, 303.
(2) Xia, Y. N.; Whitesides, G. M. *Annu. Rev. Mater. Sci.* **1998**, *28*, 153.
(3) Nie, Z. H.; Kumacheva, E. *Nat. Mater.* **2008**, *7*, 277.
(4) Xia, F.; Jiang, L. *Adv. Mater.* **2008**, *20*, 2842.
(5) Tsujii, Y.; Ohno, K.; Yamamoto, S.; Goto, A.; Fukuda, T. Structure and properties of high-density polymer brushes prepared by surface-initiated living radical polymerization. In *Surface-Initiated Polymerization I*; Advincula, R., Jordan, R., Eds.; Springer-Verlag: Berlin, 2006; Vol. 197; pp 1−46.
(6) Takei, Y. G.; Aoki, T.; Sanui, K.; Ogata, N.; Sakurai, Y.; Okanao, T. *Macromolecules* **1994**, *27*, 6163.
(7) Harnish, B.; Robinson, J. T.; Pei, Z. C.; Ramstrom, O.; Yan, M. D. *Chem. Mater.* **2005**, *17*, 4092.
(8) Minko, S.; Ionov, L.; Sydorenko, A.; Houbenov, N.; Stamm, M.; Zdyrko, B.; Klep, V.; Luzinov, I. Gradient Stimuli-Responsive Polymer Grafted Layers. In *Stimuli-Responsive Polymeric Films and Coatings*; Urban, M. W., Ed.; American Chemical Society: Washington, DC, 2005; Chapter 5, pp 68−83.
(9) Mansky, P.; Liu, Y.; Huang, E.; Russell, T. P.; Hawker, C. J. *Science* **1997**, *275*, 1458.
(10) Maeda, N.; Chen, N. H.; Tirrell, M.; Israelachvili, J. N. *Science* **2002**, *297*, 379.
(11) Klein, J.; Luckham, P. F. *Macromolecules* **1986**, *19*, 2007.
(12) Israelachvili, J.; Tandon, R. K.; White, L. R. *Nature* **1979**, *277*, 120.
(13) Klein, J.; Luckham, P. F. *Nature* **1982**, *300*, 429.
(14) Raviv, U.; Giasson, S.; Kampf, N.; Gohy, J. F.; Jerome, R.; Klein, J. *Nature* **2003**, *425*, 163.
(15) Chen, M.; Briscoe, W. H.; Armes, S. P.; Klein, J. *Science* **2009**, *323*, 1698.
(16) Sirchabesan, M.; Giasson, S. *Langmuir* **2007**, *23*, 9713.
(17) Leger, L.; Raphael, E.; Hervert, H. *Adv. Polym. Sci.* **1999**, *138*, 185.
(18) Klein, J. *Annu. Rev. Mater. Sci.* **1996**, *26*, 581.
(19) Smith, G. S.; Kuhl, T. L.; Hamilton, W. A.; Mulder, D. J.; Satija, S. *Physica B* **2006**, *385−386*, 700.
(20) Gong, J. P. *Soft Matter* **2006**, *2*, 544.
(21) Liberelle, B.; Giasson, S. *Langmuir* **2008**, *24*, 1550.
(22) Colonne, M.; Chen, Y.; Wu, K.; Freiberg, S.; Giasson, S.; Zhu, X. X. *Bioconjugate Chem.* **2007**, *18*, 999.
(23) Banquy, X.; Rabanel, J. M.; Hildgen, P.; Giasson, S. *Aust. J. Chem.* **2007**, *60*, 638.
(24) Banquy, X.; Zhu, X. X.; Giasson, S. *J. Phys. Chem. B* **2008**, *112*, 12208.
(25) Mansson, M. O.; Mosbach, K. *Methods Enzymol.* **1987**, *136*, 3.
(26) Jirku, V.; Turkova, J. *Methods Enzymol.* **1987**, *135*, 341.
(27) Prevo, B. G.; Kuncicky, D. M.; Velev, O. D. *Colloids Surf. A* **2007**, *311*, 2.
(28) Prevo, B. G.; Velev, O. D. *Langmuir* **2004**, *20*, 2099.
(29) Israelachvili, J. *J. Colloid Interface Sci.* **1973**, *44*, 259.
(30) Israelachvili, J. *Intermolecular and Surface Forces*, 2nd ed.; Academic Press: San Diego, CA, 1991.
(31) Banquy, X.; Giasson, S.; Hildgen, P.; Rabanel, J. M.; Bouchard, J. F.; Grütter, P.; Suarez, F.; Argaw, A. *Soft Matter* **2009**, *5*, 3984.
(32) Wiedemair, J.; Serpe, M. J.; Kim, J.; Masson, J. F.; Lyon, L. A.; Mizaikoff, B.; Kranz, C. *Langmuir* **2007**, *23*, 130.
(33) Tagit, O.; Tomczak, N.; Vancso, G. J. *Small* **2008**, *4*, 119.
(34) Hashmi, S. M.; Dufresne, E. R. *Soft Matter* **2009**, *5*, 3682.
(35) Liberelle, B.; Giasson, S. *Langmuir* **2008**, *24*, 1550.
(36) Rabin, Y.; Alexander, S. *Europhys. Lett.* **1990**, *13*, 49.
(37) Nordgren, N.; Rutland, M. W. *Nano Lett.* **2009**, *9*, 2984.
(38) Degennes, P. G. *Macromolecules* **1980**, *13*, 1069.
(39) Briscoe, B. J.; Evans, D. C. B. *Proc. R. Soc. London, A* **1982**, *380*, 389.
(40) Drummond, C.; Rodriguez-Hernandez, J.; Lecommandoux, S.; Richetti, P. *J. Chem. Phys.* **2007**, *126*, 12.
(41) He, G.; Robbins, M. O. *Tribol. Lett.* **2001**, *10*, 7.
(42) van der Vegte, E. W.; Subbotin, A.; Hadziioannou, G.; Ashton, P. R.; Preece, J. A. *Langmuir* **2000**, *16*, 3249.
(43) Drummond, C.; Israelachvili, J.; Richetti, P. *Phys. Rev. E* **2003**, *67*, 066110.
(44) Mazuyer, D.; Cayer-Barrioz, J.; Tonck, A.; Jarnias, F. *Langmuir* **2008**, *24*, 3857.
(45) Kurokawa, T.; Tominaga, T.; Katsuyama, Y.; Kuwabara, R.; Furukawa, H.; Osada, Y.; Gong, J. P. *Langmuir* **2005**, *21*, 8643.
(46) Charitat, T.; Joanny, J.-F. *Eur. Phys. J. E* **2000**, *3*, 369.
(47) Gong, J. P.; Osada, Y. *J. Chem. Phys.* **1998**, *109*, 8062.
(48) Schallamach, A. *Wear* **1968**, *6*, 375.
(49) Persson, B. N. J. *Phys. Rev. B* **1995**, *51*, 13568.

JP910965P